Fermi Surface Nesting and Phonon Frequency Gap Drive Anomalous Thermal Transport

Chunhua Li, Navaneetha K. Ravichandran, Lucas Lindsay, and David Broido

Phys. Rev. Lett. **121**, 175901 — Published 22 October 2018

DOI: 10.1103/PhysRevLett.121.175901

Fermi surface nesting and phonon frequency gap drive anomalous thermal transport

Chunhua Li[1], Navaneetha K. Ravichandran[1], Lucas Lindsay[2], and David Broido[1]

[1]*Department of Physics, Boston College, Chestnut Hill, Massachusetts 02467, USA*
[2]*Oak Ridge National Laboratory, Oak Ridge, Tennessee 37831, USA*

Abstract--

The lattice thermal conductivity, k_L, of typical metallic and non-metallic crystals decreases rapidly with increasing temperature because phonons interact more strongly with other phonons than they do with electrons. Using first principles calculations, we show that k_L can become nearly independent of temperature in metals that have nested Fermi surfaces and large frequency gaps between acoustic and optic phonons. Then, the interactions between phonons and electrons become much stronger than the mutual interactions between phonons, giving the fundamentally different k_L behavior. This striking trend is revealed here in the group V transition metal carbides, vanadium carbide, niobium carbide and tantalum carbide and should also occur in several of other metal compounds. This work gives insights into the physics of heat conduction in solids and identifies a new heat flow regime driven by the interplay between Fermi surfaces and phonon dispersions.

PACS: 63.20kg, 63.20.kd, 63.20.dk, 65.40-b

In non-magnetic electrical insulators, heat is carried by phonons. Intrinsic thermal resistance arises from mutual interactions among phonons caused by the anharmonicity of the interatomic potential [1, 2]. Around and above room temperature, the lattice thermal conductivity, k_L, decreases sharply with temperature, with $k_L \sim 1/T$ above the Debye temperature of the material. In metals heat is carried by electrons and phonons, and their mutual interactions add to the lattice thermal resistance beyond that from phonon-phonon scattering alone. Heat conduction in metals was described qualitatively by Makinson eighty years ago [3]. He showed that the contribution to thermal conduction from phonons involves a temperature dependent competition between phonon-phonon and phonon-electron interactions, with the former dominating the behavior at high T and the latter dominating at low T. Specifically, k_L limited only by phonon-electron scattering tends to zero at low T and becomes temperature independent at high T. Since k_L limited only by anharmonic phonon-phonon interactions decreases monotonically with increasing T, a temperature cross-over occurs below which phonon-electron scattering dominates and above which phonon-phonon scattering dominates [2, 3]. Simple estimates [2] show that this cross-over should occur well below room temperature so that around and above room temperature phonon-phonon scattering should be far stronger than phonon-electron scattering. Such behavior has been confirmed in recent *ab initio* calculations of k_L for the common metals, Al, Cu, Ag, Au, Ni, Pt [4, 5]. It thus appears that the strong monotonic decrease in k_L with increasing T above room temperature is a universal behavior of all non-magnetic crystals, regardless of whether they are metallic or non-metallic.

In this Letter, we show using a first principles theory that strikingly different temperature dependence of k_L can occur in metallic compounds that combine nested Fermi surfaces with specific vibrational properties of the atomic lattice. Fermi surface nesting (FSN) contributes to

strong electron-phonon interactions, and it has been the subject of intense interest for decades in the study of strongly correlated electron systems and phenomena such as charge density waves and superconductivity [6-8]. To our knowledge, the influence of FSN on heat conduction has not been rigorously investigated before. We demonstrate that FSN combined with particular phonon properties can yield anomalously weak phonon-phonon interactions *simultaneously* with strong phonon-electron interactions, which is opposite to the typical behavior. This interplay between the structure of the Fermi surface and the vibrational properties of the atomic lattice makes k_L nearly temperature independent around room temperature and extending well above it.

To demonstrate the effect of this novel interplay between the electronic and phononic energy spectra, we present results for two classes of transition metal carbides (TMCs). We show that the unusual temperature independence occurs in the group V TMCs, VC, NbC, and TaC, where Fermi surface nesting is known to occur. In contrast, the group IV TMCs, TiC, ZrC, and HfC, which do not have nested Fermi surfaces, show the typical behavior, $k_L \sim 1/T$.

***First principles theory*:** We have implemented a first principles approach to calculate the k_L of TMCs. These materials crystallize in the rock salt structure and are known as refractory compounds because of their unusual hardness and high melting points [9-11], which stem from strong covalent bonding [12]. Phonons are taken to scatter (i) with other phonons; three-phonon scattering is the lowest-order intrinsic process; (ii) from isotopes; these produce a mass disorder that scatters phonons [13]; and (iii) with electrons. Harmonic interatomic force constants (IFCs) are calculated using Density Functional Perturbation Theory (DFPT) [14]. From these, phonon modes, acoustic velocities and phonon-isotope scattering rates [13] are obtained. Anharmonic IFCs are calculated using a supercell approach, from which phonon-phonon scattering rates are determined [15]. Thermal expansion is incorporated within the quasi-harmonic approximation.

Further details are given in the Supplementary Materials [16]. We note that while FSN can indicate strong electron correlations, such as occurs in TaS_2 and $TaSe_2$, this does not appear to be the case for the TMCs whose properties have been accurately described by density functional theory [23, 24] without including strong electron correlation corrections using e.g. DFT+U or dynamical mean field theory.

The scattering rates of phonons by electrons are [2, 25-28]:

$$\frac{1}{\tau^{\mathrm{L}}_{\mathrm{ph-el}}} = \frac{2\pi\Omega_0}{\hbar}\sum_{mn}\int \frac{\mathrm{d}\mathbf{k}}{4\pi^3}\left|g^{\mathrm{SE}}_{nm,j}(\mathbf{k},\mathbf{q})\right|^2\left(f_0(\varepsilon_{n\mathbf{k}}) - f_0(\varepsilon_{m\mathbf{k+q}})\right)\delta\left(\varepsilon_{m\mathbf{k+q}} - \varepsilon_{n\mathbf{k}} - \hbar\omega_{j\mathbf{q}}\right) \qquad (1)$$

Here, Ω_0 is the volume of the unit cell, $\varepsilon_{n\mathbf{k}}$ and $\varepsilon_{m\mathbf{k+q}}$ are electron energies in the initial (n,$\mathbf{k}$) and the final (m,$\mathbf{k+q}$) states, $\hbar\omega_{j\mathbf{q}}$ is the energy of a phonon with wavevector $\mathbf{q}$ and polarization, j, the sums are over the electron bands, n, m; f_0 is the Fermi distribution, and $g^{\mathrm{SE}}_{nm,j}(\mathbf{k},\mathbf{q})$ is the electron-phonon scattering matrix element. IFCs, phonon frequencies and electron energies are calculated using the Quantum Espresso package [29, 30] with norm-conserving pseudopotentials in the generalized gradient approximation. The electron-phonon matrix elements, $g^{\mathrm{SE}}_{nm,j}(\mathbf{k},\mathbf{q})$, are evaluated *ab initio* using the Electron-Phonon Wannier code [25-27, 31]. The total phonon scattering rates are obtained from Mathiessen's rule: $1/\tau^{\mathrm{L}}_{\mathrm{tot}} = 1/\tau^{\mathrm{L}}_{\mathrm{ph-ph}} + 1/\tau^{\mathrm{L}}_{\mathrm{ph-iso}} + 1/\tau^{\mathrm{L}}_{\mathrm{ph-el}}$, where $1/\tau^{\mathrm{L}}_{\mathrm{ph-ph}}$ and $1/\tau^{\mathrm{L}}_{\mathrm{ph-iso}}$ are the three-phonon and phonon-isotope scattering rates, respectively, determined *ab initio*. For further details see Ref. 16.

The lattice thermal conductivity, k_{L}, can be expressed as

$$k^{\alpha\beta}_{\mathrm{L}} = \sum_{\lambda} C_\lambda v_{\lambda\alpha} v_{\lambda\beta} \tau^{\mathrm{L}}_{\lambda\beta} \qquad (2)$$

where the sum is over all phonon modes λ=(j, $\mathbf{q}$), $C_\lambda = \hbar\omega_\lambda(\partial n_\lambda^0 / \partial T)/V$ is the specific heat capacity per phonon mode, n_λ^0 is the Bose factor at temperature T, $\mathbf{v}_\lambda$ is the velocity of mode λ, α and β are Cartesian components, and V is the crystal volume. The phonon transport lifetime in mode λ, $\tau_{\lambda\beta}^{\mathrm{L}}$, is obtained by solving the Peierls-Boltzmann transport equation (PBE) for the non-equilibrium phonon distribution that results from a small temperature gradient applied along crystallographic axis direction β. Solution of the PBE is accomplished using an iterative approach described previously [32-35]. The solution incorporates the quantum-mechanical scattering rates, and it goes beyond the commonly used relaxation time approximation in properly accounting for the difference between momentum-conserving Normal phonon-phonon scattering processes, and resistive Umklapp phonon-phonon processes [1, 2].

***Anomalous thermal transport*:** Figure 1a shows the calculated Fermi surface for NbC. The six arms of this surface have roughly square cross-section resulting in large parallel regions connected by specific phonon wave vectors, which defines some of the nesting. In fact, Weber [31] showed that a roughly cubic surface of nesting vectors exists in the phonon Brillouin zone. There are three nesting vectors along [100] (red arrow in Fig. 1a), [110] and [111] high symmetry directions. The nesting regions give rise to strong interactions between electrons and phonons, which renormalize some phonon energies producing phonon anomalies [23, 24, 37-40]. Fig. 2a shows the calculated phonon dispersions for NbC illustrating these well-known phonon anomalies [41].

Several features are responsible for the weak phonon-phonon scattering. To understand these, we first note that heat is carried primarily by the acoustic phonons. Intrinsic thermal resistance arises from scattering between three acoustic phonons (*aaa*), two acoustic phonons and an optic

phonon (*aao*), or an acoustic phonon and two optic phonons (*aoo*). The large mass of Nb atoms (92.91 amu) compared to C atoms (12.01 amu) produces a large frequency gap between acoustic and optic phonons, which forbids *aao* processes since they cannot satisfy energy conservation [43]. The narrow bandwidth of the optic phonon branches restricts *aoo* processes to the region of low frequencies [44] where their scattering rates are weaker than *aaa* processes. Furthermore, Nb is isotopically pure. As a result, scattering of acoustic phonons by isotopic mass disorder is weak [13, 45]. Thus, absent phonon-electron scattering, k_L is limited primarily by *aaa* scattering. Then, the bunched together regions of acoustic branches caused by these phonon anomalies severely restricts the phase space for *aaa* scattering, as has been pointed out previously [43]. These combined features give weak phonon-phonon and phonon-isotope scattering rates for the heat-carrying acoustic phonons. We note that higher-order four-phonon scattering has recently been found to be important in non-metallic crystals with large frequency gaps between acoustic and optic phonons, such as BAs [46]. However, we expect that it would be much weaker than the phonon-electron scattering found here in NbC, VC and TaC [16].

To highlight these contrasting behaviors, the phonon-phonon and phonon-electron scattering rates for NbC at 300K are shown in Fig. 3a for the acoustic phonons. At low frequency, phonon-phonon scattering is stronger than phonon-electron scattering. With increasing frequency, a striking drop occurs in the phonon-phonon scattering rates (in the 4 to 8 THz regime), resulting from the small phase space for phonon-phonon scattering in this region. In the same frequency range, a large increase in the phonon-electron scattering rates is seen, driven by the FSN. Similar behavior of the Fermi surfaces, phonon dispersions, phonon-phonon and phonon-electron scattering rates is found for VC and TaC [16].

The lattice thermal conductivity of NbC is shown in Fig. 4 for two cases: (i) limited by phonon-phonon and phonon-isotope scattering alone (dashed blue curve); (ii) including phonon-phonon, phonon-isotope and phonon-electron scattering (solid blue curve). For case (i), k_L is extremely high, over 3000$Wm^{-1}K^{-1}$ at 300K. These k_L values are comparable to or higher than the highest values achieved for a bulk crystal (i.e. diamond) over the same temperature range [47-49]. Including phonon-electron scattering, case (ii), decreases k_L by three orders of magnitude. This large reduction reflects the much stronger phonon-electron scattering compared to phonon-phonon scattering in the frequency region of the nesting vectors, as seen in Fig. 3a. This results in a near temperature independence of k_L over the 300K-1000K range.

To contrast this unusual behavior for the group V TMCs, we have performed calculations for the group IV TMCs: TiC, ZrC and HfC. Figs. 1b and 2b show the Fermi surface and phonon dispersions for TiC. Some nesting appears to occur for small wave vectors [23] that may cause softening of the optic phonons around the Γ point. However, TiC shows no anomalies in the acoustic phonon spectrum. Figure 3b shows the phonon-phonon and phonon-electron scattering rates for TiC at 300K. The phonon-phonon scattering rates for TiC are generally much larger than the phonon-electron scattering rates over the full acoustic phonon frequency range. As a result, for TiC the k_L neglecting phonon-electron scattering is seen to be almost the same as that including it, as shown in Fig. 4. The total k_L decreases roughly as *1/T* around and above 300K, consistent with the temperature dependence of k_L in typical crystalline metals and non-metals. Similar behavior is found for ZrC and HfC [16].

Figure 5 compares k_L for the six TMCs as a function of *T*. Consistent with the above discussion the k_L values decrease rapidly with *T* for all group IV TMCs, while those for the group V TMCs are almost temperature independent over the same *T* range. Around room

temperature, group IV TMCs have far larger k_L than those of the group V TMCs, while at high T the k_L for the group IV TMCs are similar to those for the group V TMCs.

Experimental verification of the anomalous temperature dependence of k_L predicted here for the group V TMCs requires high quality samples. TMCs and TM nitrides typically have large concentrations of non-metal (C and N) vacancies [9-12], which would strongly suppress the intrinsic k_L and make it temperature independent thereby masking the anomalous behavior. Recently, high quality growth of thin films of stoichiometric vanadium nitride (VN) has been achieved on MgO substrates [51]. The k_L extracted from measurements of the total thermal conductivity of VN [52] using the Wiedemann-Franz law and simple models for electronic structure and transport showed a relatively weak dependence on temperature in the 300K-550K range. As was pointed out in Ref. 52, VN should have strong electron-phonon scattering given its rather high superconducting transition temperature ~9K [9]. Since our computational approach does not determine temperature dependent IFCs, we are not able to capture the phonon behavior of VN in the rock salt phase and so cannot directly calculate k_L to compare to the measured data. Instead, we have calculated the Fermi surface of VN in the rock salt structure [16], which indeed shows nested regions whose nesting vector corresponds to the phonon anomaly around the X point observed in the measured phonon dispersions [52]. However, the frequency gap between acoustic and optic phonons [53] is not large enough to freeze out *aao* scattering processes. This suggests that phonon-phonon scattering is not weak in VN. In fact, extrapolating the roughly linear k_L found in Ref. 52 to higher T predicts a factor of two reduction in k_L at 1000K compared to that at 300K, far larger than the corresponding reductions in the calculated k_L values of VC, NbC and TaC.

The electronic and phonon properties responsible for the anomalously weak T dependence of k_L found here in the group V TMCs occur in other compounds. Specifically, ZrN and HfN both show FSN and phonon anomalies [24, 54] and their electron-phonon coupling constants are large [24]. Also, their phonon dispersions show large frequency gaps between acoustic and optic phonons. As a result, we speculate that near T independent k_L should also occur in these compounds over a similarly large T range around and above room temperature. TiN, ScC and YC also exhibit nesting [24, 55] and have larger electron-phonon coupling constants [24] suggesting that electron-phonon scattering should be strong. However, their frequency gaps between acoustic and optic phonons are not sufficiently large to freeze out the scattering between the heat-carrying acoustic phonons and optic phonons. Therefore, we predict a stronger T dependence of k_L in these compounds above 300K than should occur in VC, NbC, TaC, ZrN or HfN, but still weaker than the typical phonon-phonon scattering dominated behavior, qualitatively similar to that found in VN [52]. We note that large suppression of k_L was recently predicted for highly doped Si where phonon-electron and phonon-phonon scattering rates were found to be similar for carrier densities around 10^{21} cm^{-3} [56].

To summarize, employing first principles calculations, we demonstrate that in metals with nested Fermi surfaces and large frequency gaps between heat-carrying acoustic phonons and optic phonons an unusual combination of weak phonon-phonon interactions and strong electron-phonon interactions occurs. This combination, the reverse of the typical behavior in both metallic and non-metallic crystals, is predicted for several transition metal carbide (VC, NbC and TaC) and nitride (ZrN and HfN) compounds. It gives a nearly temperature independent lattice thermal conductivity to well above room temperature in striking contrast to the rapid decrease of lattice thermal conductivity with temperature normally found in crystalline solids. This work

gives new insights into heat conduction in solids and identifies an anomalous regime of transport behavior whose experimental verification should be possible through growth and characterization of high quality crystals of the identified metal compounds.

Acknowledgements:

C. L. and D. B. acknowledge support from the National Science Foundation under grant No. 1402949. C. L., N. K. R. and D. B. acknowledge support from the Office of Naval Research MURI, Grant No. N00014-16-1-2436. L.L. acknowledges support from the U.S. Department of Energy, Office of Science, Office of Basic Energy Sciences, Materials Sciences and Engineering Division for work done at ORNL. The computational part of this research used resources of the the Extreme Science and Engineering Discovery Environment (XSEDE), which is supported by National Science Foundation grant numbers TG-ASC160070 and ACI-1548562, and the Boston College linux clusters.

References

[1] R. E. Peierls, *Quantum Theory of Solids*, (Oxford at The Clarendon Press, 1955).

[2] J. M. Ziman, *Electrons and Phonons* (Oxford University Press, London, 1960).

[3] R.E. B. Makinson, *The thermal conductivity of metals*, Mathematical Proceedings of the Cambridge Philosophical Society **34**, 474-497 (1938).

[4] Ankit Jain and Alan J. H. McGaughey, *Thermal transport by phonons and electrons in aluminum, silver, and gold from first principles*, Physical Review B **93**, 081206(R) (2016).

[5] Yan Wang, Zexi Lu, and Xiulin Ruan, *First principles calculation of lattice thermal conductivity of metals considering phonon-phonon and phonon-electron scattering*, Journal of Applied Physics **119**, 225109 (2016).

[6] Patrick A. Lee, Naoto Nagaosa, and Xiao-Gang Wen, Doping a Mott insulator: Physics of high-temperature superconductivity, Reviews of Modern Physics 78, 17-85 (2006).

[7] M.-H. Whangbo, E. Canadell, P. Foury and J.-P. Pouget, *Hidden Fermi Surface Nesting and Charge Density Wave Instability in Low-Dimensional Metals*, Science 252, 96-98 (1991).

[8] Feliciano Giustino, *Electron-phonon interactions from first principles*, Reviews of Modern Physics 89, 015003 (2017).

[9] Louis E. Toth, Ed., *Refractory Materials A Series of Monographs, Volume 7: Transition Metal Carbides and Nitrides* (Academic Press, New York, 1971).

[10] Hugh O. Pierson, *Handbook of Refractory Carbides and Nitrides* (Noyes Publications, New Jersey, 1996).

[11] Yukinobu Kumashiro, Ed., *Electric Refractory Materials* (Marcel Dekker, Inc, New York, 2000).

[12] V. A. Gubanov, A. L. Ivanovsky and V. P. Zhukov, Electronic Structure of Refractory Carbides and Nitrides (Cambridge University Press, 2005).

[13] S.-i. Tamura, *Isotope scattering of large wave-vector phonons of GaAs and InSb: Deformation-dipole and overlap shell models*, Physical Review B **30**, 849-854 (1984).

[14] [S. Baroni, S. Gironcoli, A. D. Corso, and P. Giannozzi, *Phonons and related crystal properties from density-functional perturbation theory*, Reviews of Modern Physics **73**, 515-562 (2001).

[15] K. Esfarjani and H. T. Stokes, *Method to extract anharmonic force constants from first principles calculations*, Phys. Rev. B 77, 144112 (2008).

[16] See Supplementary Materials at http://link.aps.org… for computational details of phonon dispersions, three-phonon, phonon-electron and phonon-isotope scattering rates, corroboration of nesting vectors with location of phonon anomalies, consideration of four-phonon scattering, plots of Fermi surfaces, phonon dispersions and three-phonon scattering rates for VC, TaC, ZrC, and HfC, and Fermi surface of VN, which includes Refs. [17-22].

[17] John P. Perdew, Kieron Burke, and Matthias Ernzerhof, Phys. Rev. Lett. 77, 3865 (1996).

[18] Materials Science and Engineering B 148 (2008) 69–72.

[19] A. A. Maradudin, E. W. Montroll, and G. H. Weiss, Theory of Lattice Dynamics in the Harmonic Approximations Academic, New York, 1963d, Vol. 3 of Solid-state physics.

[20] W. Li, L. Lindsay, D. Broido, D. A. Stewart, N. Mingo, *Thermal conductivity of bulk and nanowire $Mg_2Si_xSn_{1-x}$ alloys from first principles*, Physical Review B 86, 174307 (2012).

[21] Junichiro Shiomi, Keivan Esfarjani, and Gang Chen, *Thermal conductivity of half-Heusler compounds from first-principles calculations*, Physical Review B 84, 104302 (2011).

[22] Dimitris Zaharioudakis, *Tetrahedron methods for Brillouin zone integration*, Computer Physics Communications **157**, 17–31 (2004).

[23] Jesse Noffsinger, Feliciano Giustino, Steven G. Louie, and Marvin L. Cohen, *First-principles study of superconductivity and Fermi-surface nesting in ultrahard transition metal carbides*, Physical Review B **77** 180507(R) (2008).

[24] E. I. Isaev, S. I. Simak and I. A. Abrikosov, R. Ahuja, Yu. Kh. Vekilov, M. I. Katsnelson, A. I. Lichtenstein and B. Johansson, *Phonon related properties of transition metals, their carbides, and nitrides: A first principles study*, Journal of Applied Physics **101** 123519 (2007).

[25] Feliciano Giustino, Marvin L. Cohen, and Steven G. Louie, *Electron-phonon interaction using Wannier functions*, Physical Review B **76**, 165108 (2007).

[26] Jesse Noffsinger, Feliciano Giustino, Brad D. Malone, Cheol-Hwan Park, Steven G. Louie, Marvin L. Cohen, *EPW: A program for calculating the electron–phonon coupling using maximally localized Wannier functions*, Computer Physics Communications **181**, 2140-2148 (2010).

[27] S. Poncé, E. R. Margine, C. Verdi, F. Giustino, *EPW: Electron–phonon coupling, transport and superconducting properties using maximally localized Wannier functions*, Computer Physics Communications **209**, 116-133 (2016).

[28] Henrik Smith and Hojgaard Jensen, *Tranport Phenomena*, (Clarendon Press, Oxford 1989).

[29] P. Giannozzi et al., *QUANTUM ESPRESSO: a modular and open-source software project for quantum simulations of materials***,** J. Phys. Cond. Matt. **21**, 395502 (2009).

[30] P. Giannozzi et. al., *Advanced capabilities for materials modelling with Quantum ESPRESSO,* J. Phys. Cond. Matt. **29**, 465901 (2017).

[31] http://epw.org.uk/Main/HomePage

[32] M. Omini, A. Sparavigna, *An iterative approach to the phonon Boltzmann equation in the theory of thermal conductivity*, Physica B: Condensed Matter 212, 101-112 (1995).

[33] D. A. Broido, A. Ward, and N. Mingo, Lattice thermal conductivity of silicon from empirical interatomic potentials. Physical Review B **72**, 014308 (2005).

[34] D. A. Broido, D. A., M. Malorny, G. Birner, N. Mingo, and D. A. Stewart, *Intrinsic lattice thermal conductivity of semiconductors from first principles*, Applied Physics Letters 91, 231922 (2007).

[35] W. Li, J. Carrete, N. Katcho, and N. Mingo, ShengBTE: A solver of the Boltzmann transport equation for phonons. Computer Physics Communications 185, 1747-1758 (2014).

[36] A. Kokalj, *XCrySDen—a new program for displaying crystalline structures and electron densities***,** J. Mol. Graph. Model. 17, 176-179 (1999).

[37] W. Weber, *Lattice Dynamics of Transition-Metal Carbides*, Physical Review B **8**, 5082-5092 (1973).

[38] B.M. Klein, L.L. Boyer and D.A. Papaconstantopoulos, *On the relationship between the phonon anomalies and the ab initio calculated Fermi surfaces of TaC and NbC*, Solid State Communications, **20**, 937-940 (1976).

[39] A. Nørlund Christensen, W. Kress, M. Miura, and N. Lehner, *Phonon anomalies in transition-metal nitrides: HfN*, Physical Review B **28**, 977-981 (1983).

[40] H. G. Smith, *Phonon Anomalies in Transition-Metal Carbides*, Physical Review Letters **29**, 353-354 (1972).

[41] Correspondence between the locations of the phonon anomalies and the nesting vectors is shown in Ref. 16.

[42] H. G. Smith and W. Gläzer, in Proceedings of the International Conference on Phonons, Rennes, France, July 1971, edited by M. A. Nusimovici (Flammaron Sciences, Paris, 1971).

[43] L. Lindsay, D. A. Broido, and T. L. Reinecke, *First-Principles Determination of Ultrahigh Thermal Conductivity of Boron Arsenide: A Competitor for Diamond?*, Physical Review Letters **111**, 025901 (2013).

[44] S. Mukhopadhyay, L. Lindsay, and D. S. Parker, *Optic phonon bandwidth and lattice thermal conductivity: The case of Li2X (X = O, S, Se, Te)*, Physical Review B **93**, 224301 (2016).

[45] M. Lax, P. Hu, and V. Narayanamurti, *Spontaneous phonon decay selection rule: N and U processes*, Physical Review B **23**, 3095-3097 (1981).

[46] Tianli Feng, Lucas Lindsay, and Xiulin Ruan, *Four-phonon scattering significantly reduces intrinsic thermal conductivity of solids*, Phys. Rev. B **96**, 16201 (R) (2017).

[47] D. G. Onn, A. Witek, Y. Z. Qiu, T. R. Anthony, and W. F. Banholzer, *Some aspects of the thermal conductivity of isotopically enriched diamond single crystal,* Physical Review Letters **68**, 2806-2809 (1992).

[48] L. Wei, P. K. Kuo, R. L. Thomas, T. R. Anthony, and W. F. Banholzer, *Thermal conductivity of isotopically modified single crystal diamond*, Physical Review Letters **70**, 3764-3767 (1993).

[49] J. R. Olson, R. O. Pohl, J. W. Vandersande, A. Zoltan, T. R. Anthony and W. F. Banholzer, *Thermal conductivity of diamond between 170 and 1200 K and the isotope effect*, Physical Review B **47**, 14850-14856 (1993).

[50] L. Pintschovius, W. Reichardt, and B. Scheerer, *Lattice dynamics of TiC*, J. Phys. C **11**, 1557 (1978).

[51] A. B. Mei, O. Hellman, N. Wireklint, C. M. Schlepütz, D. G. Sangiovanni, B. Alling, A. Rockett, L. Hultman, I. Petrov, and J. E. Greene, *Dynamic and structural stability of cubic vanadium nitride*, Physical Review B **91**, 054101 (2015).

[52] Qiye Zheng, Antonio B. Mei, Mohit Tuteja, Davide G. Sangiovanni, Lars Hultman, Ivan Petrov, J. E. Greene, and David G. Cahill, *Phonon and electron contributions to the thermal conductivity of VNx epitaxial layers*, Phys. Rev. Mat. **1**, 065002 (2017).

[53] W. Weber, P. Roedhammer, L. Pintschovius, W. Reichardt, F. Gompf and A. N. Christensen, *Phonon Anomalies in VN and Their Electronic Origin*, Phys. Rev. Lett. **43**, 868-871 (1979).

[54] A. N. Christensen, O. W. Dietrich, W. Kress and W. D. Teuchert, *Phonon anomalies in transition-metal nitrides: ZrN*, Physical Review B **19**, 5699-5703 (1979).

[55] W. Kress, P. Roedhammer, H. Bilz, W. D. Teuchert, and A. N. Christensen, *Phonon anomalies in transition-metal nitrides: TiN*, Phys. Rev. B **17**, 111-113 (1978).

[56] Bolin Liao, Bo Qiu, Jiawei Zhou, Samuel Huberman, Keivan Esfarjani, and Gang Chen, *Significant Reduction of Lattice Thermal Conductivity by the Electron-PhononInteraction in Silicon with High Carrier Concentrations: A First-Principles Study*, Phys. Rev. Lett. **114** 115901 (2015).

Figure Captions

Figure 1 Fermi surface of (a) NbC and (b) TiC calculated from first principles. Images prepared using XCrySDen [36]. The red arrows show the three nesting vectors with lengths 0.66 (in units of $2\pi / a$) along Γ-X, 0.71 along Γ-K and at the L point for NbC. Possible nesting vector for TiC also shown.

Figure 2 Phonon dispersions of (a) NbC and (b) TiC calculated from first principles and compared to measured data from Ref. 42 and Ref. 50, respectively. Blue arrows in (a) show the phonon anomalies for NbC. No anomalies occur for TiC acoustic phonons.

Figure 3 Comparison of phonon-phonon (blue points) and phonon-electron (red points) scattering rates for (a) NbC and (b) TiC at 300K.

Figure 4 Lattice thermal conductivity, k_L, as a function of T for NbC limited by (i) phonon-phonon and phonon-isotope scattering (dashed blue curve), (ii) phonon-phonon, phonon-isotope and phonon-electron scattering (solid blue curve). Same for TiC with red curves.

Figure 5 Lattice thermal conductivity as a function of temperature for the group IV transition metal carbides, TiC, ZrC and HfC (dashed curves), which show strong temperature dependence, and for the group V transition metal carbides, VC, NbC and TaC, which show very little temperature dependence.

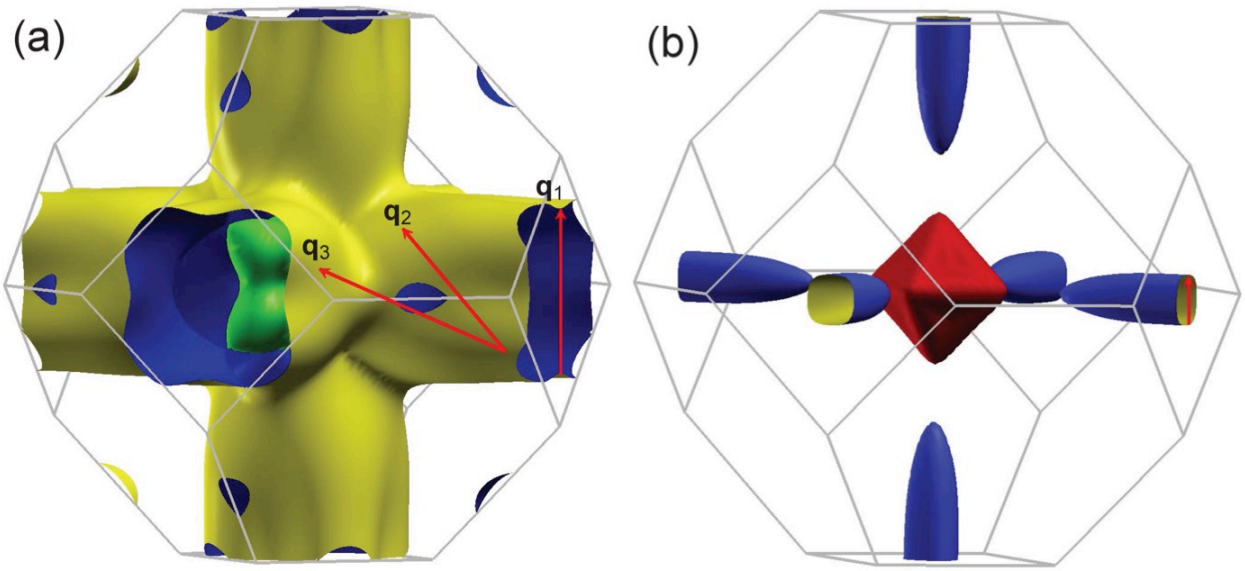

Figure 1

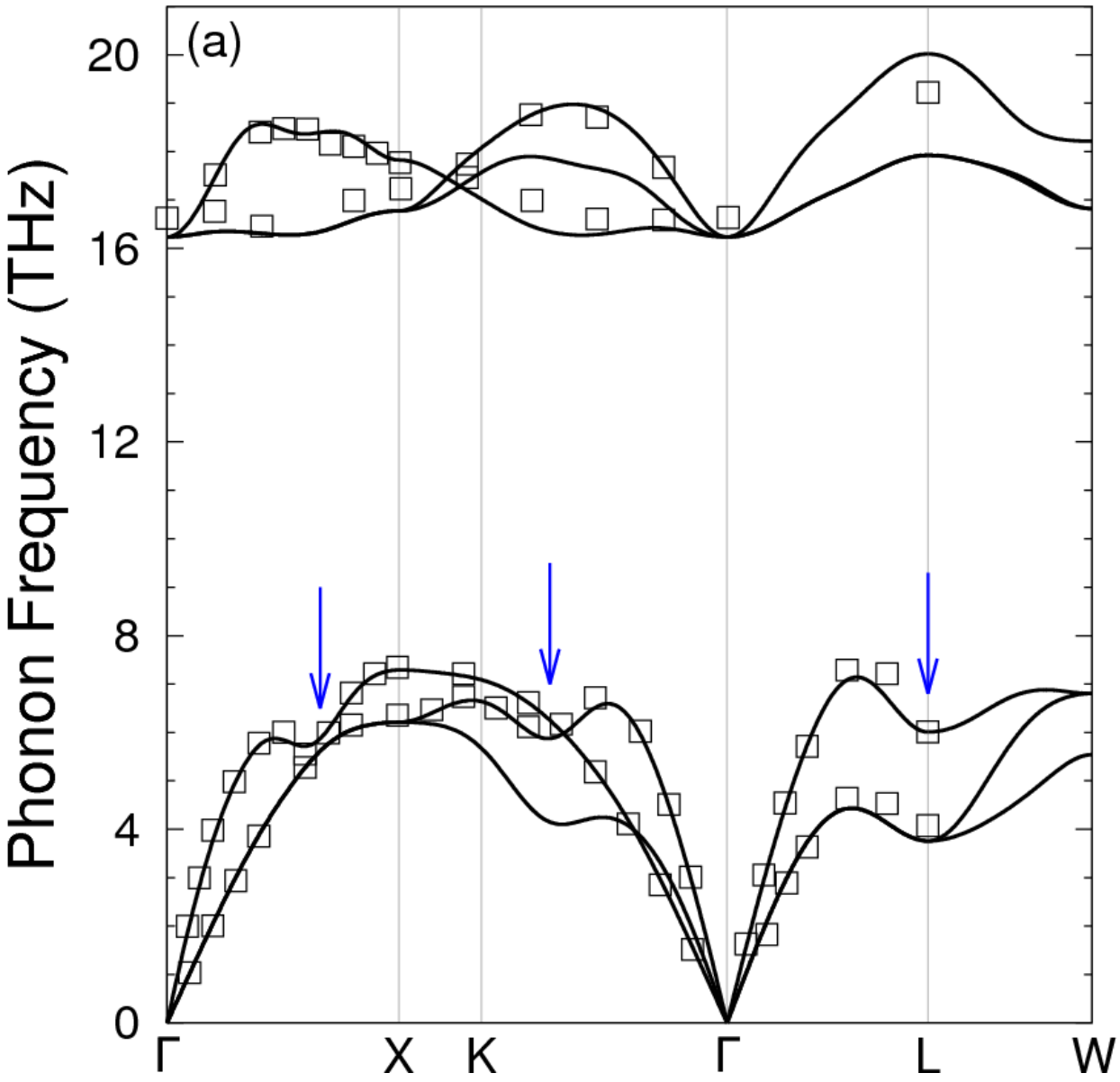

Figure 2a

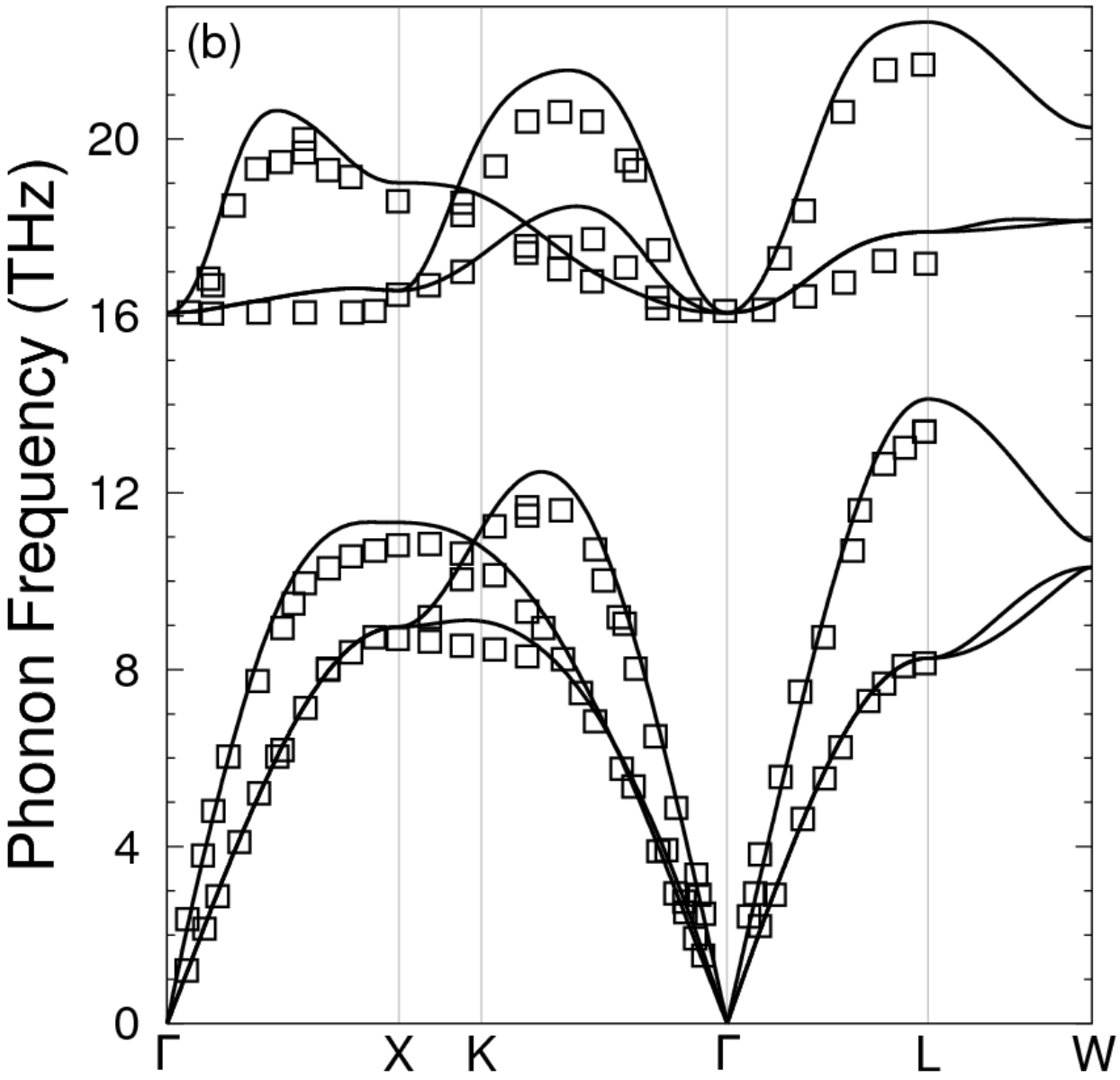

Figure 2b

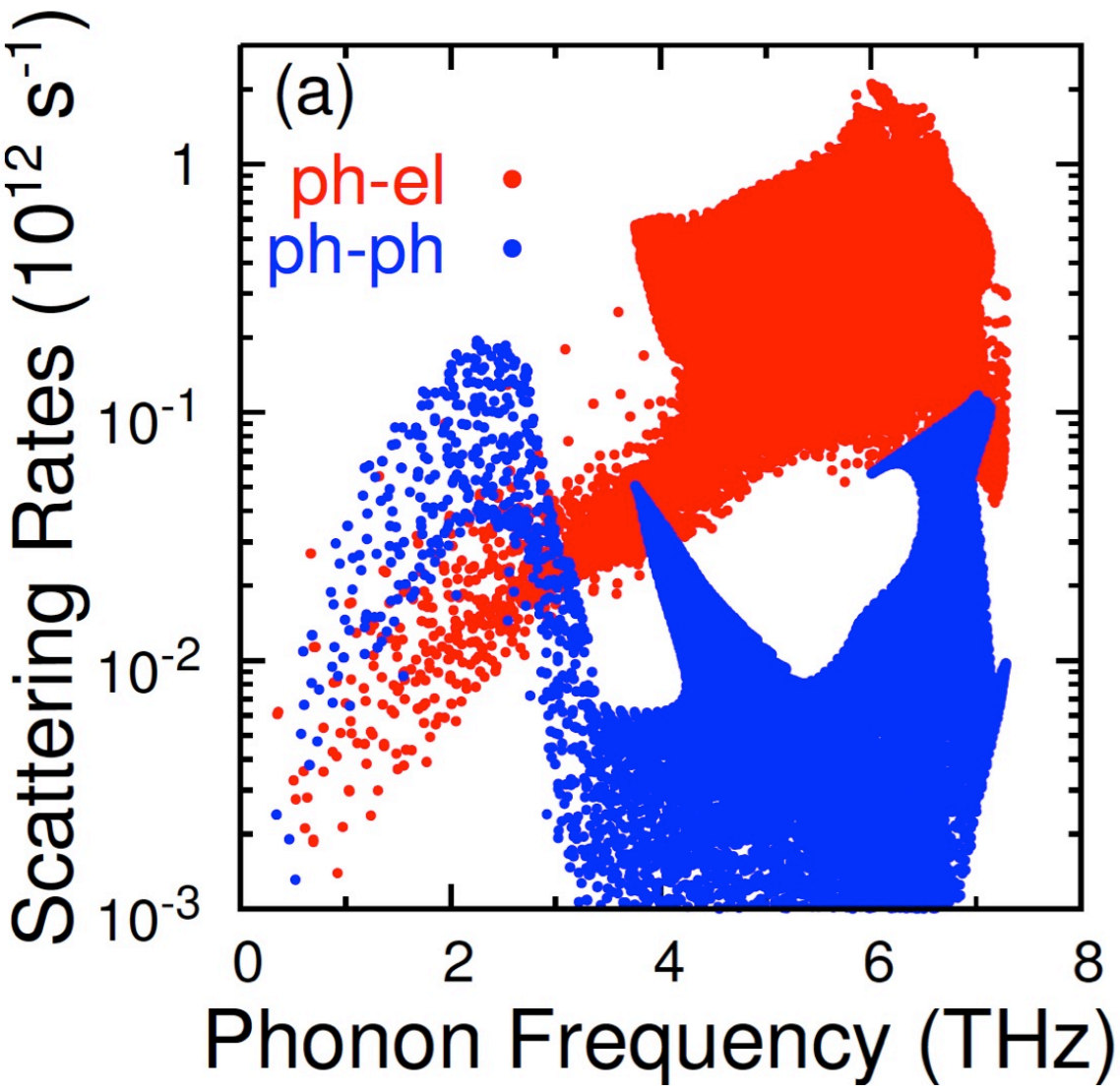
(a)
ph-el
ph-ph
Scattering Rates (10^{12} s^{-1})
1
10^{-1}
10^{-2}
10^{-3}
0
2
4
6
8
Phonon Frequency (THz)

Figure 3a

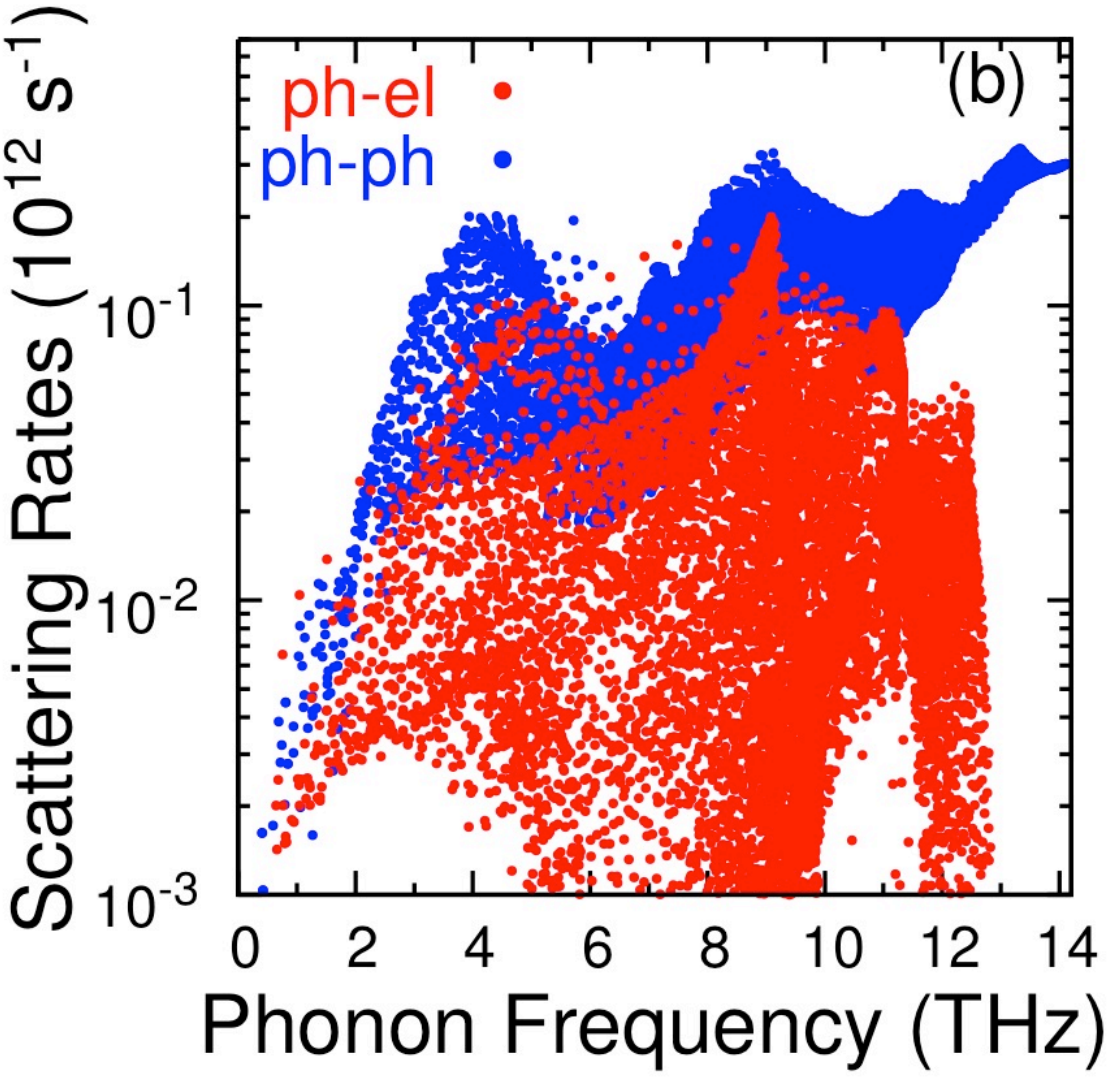
ph-el
ph-ph
(b)
Scattering Rates (10^{12} s^{-1})
10^{-1}
10^{-2}
10^{-3}
0
2
4
6
8
10
12
14
Phonon Frequency (THz)

Figure 3b

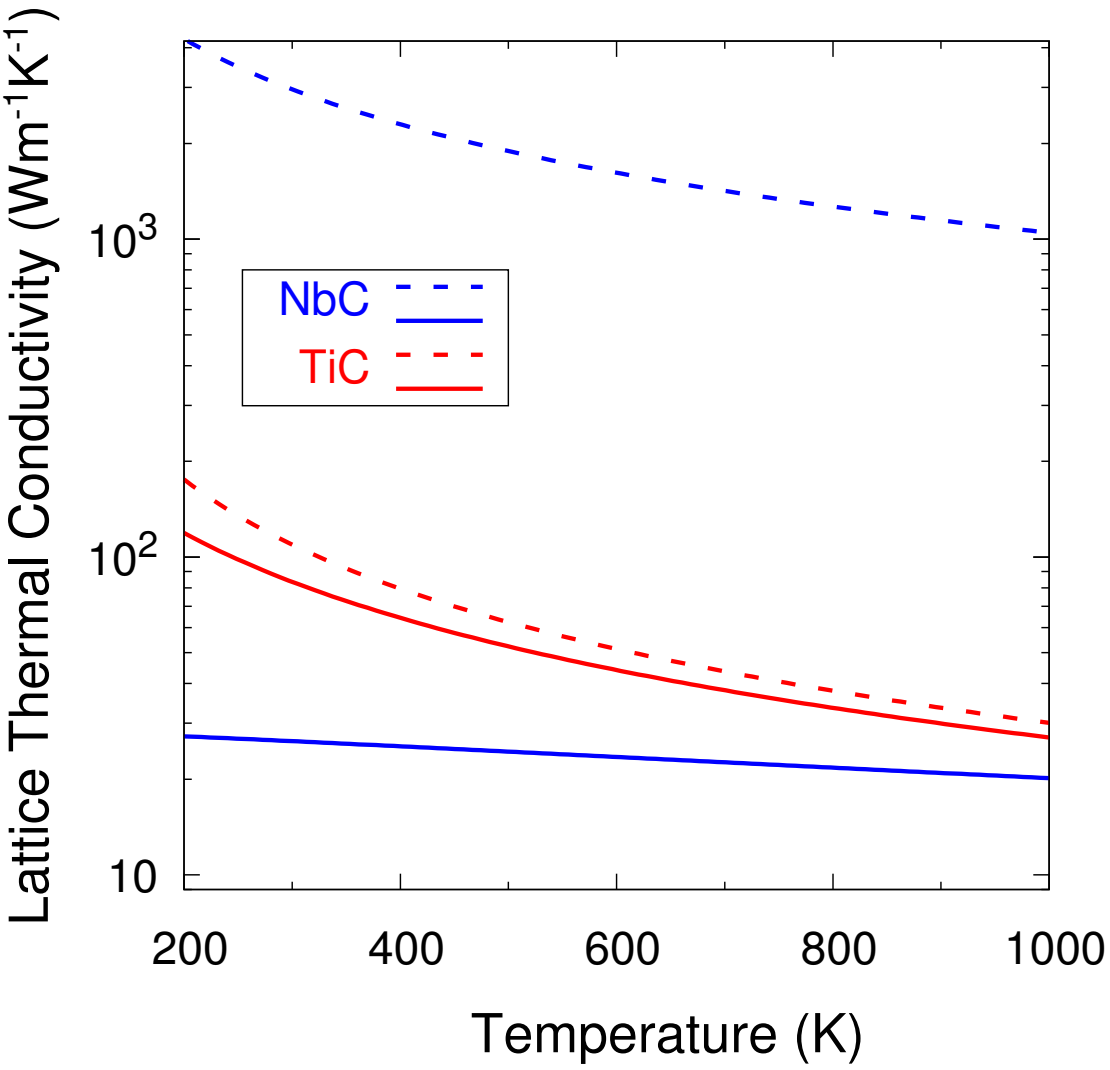
Lattice Thermal Conductivity (Wm-1K-1)
10
10^2
10^3
200
400
600
800
1000
Temperature (K)
NbC
TiC
Figure 4

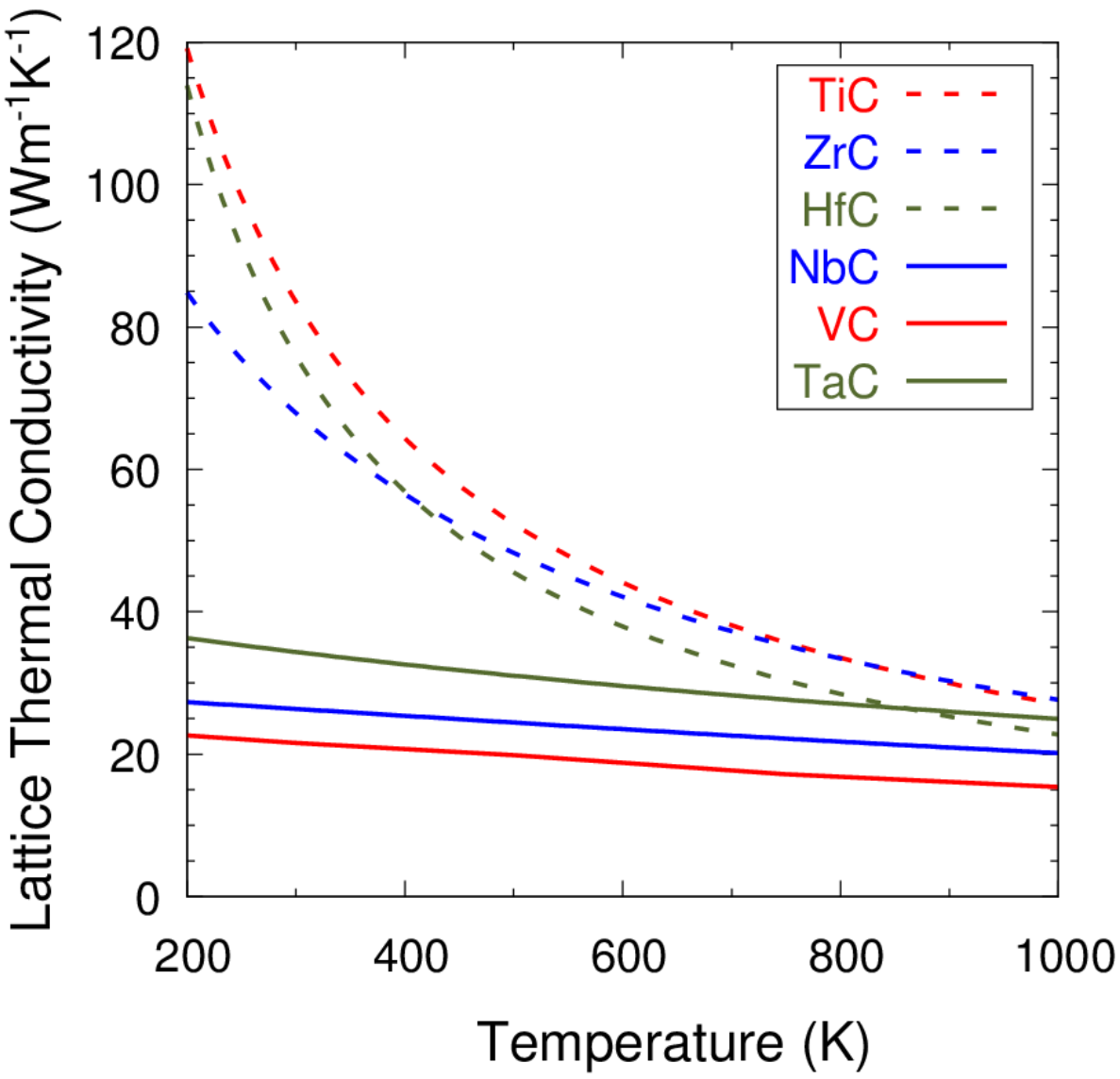
Lattice Thermal Conductivity (Wm-1K-1)
120
100
80
60
40
20
0
200
400
600
800
1000
Temperature (K)
TiC
ZrC
HfC
NbC
VC
TaC
Figure 5